Copyright © 2005 by ABCM

TURBULENT IMPINGING JET IN A CYLINDRICAL ENCLOSURE WITH A POROUS LAYER AT THE BOTTOM

Daniel R. Graminho[1]
Marcelo J.S. De-Lemos[2]
Departamento de Energia - IEME
Instituto Tecnológico de Aeronáutica - ITA
12228-900 - São José dos Campos - SP, Brazil
[1]graminho@mec.ita.br
[2]delemos@ita.br

Abstract*. Impinging jets are widely used in industry to enhance local heat transfer and drying coefficients. The addition of a porous medium contributes to a better fluid flow distribution, which favors many engineering applications. Inspired by this, the present work shows numerical results for a turbulent impinging jet against a cylindrical enclosure with and without a porous layer. The macroscopic time-average equations for mass, momentum and energy are obtained based on the Double Decomposition concept (spatial deviations and temporal fluctuations).The numerical technique employed for discretizing the governing equations is the control volume method with a boundary-fitted non-orthogonal coordinate system. The SIMPLE algorithm is used to handle the pressure-velocity coupling. For numerical solution, a structured computational grid is used, refined at the incidence region.*

Keywords*. Porous Media, Numerical Solution, Turbulent Flow, Impinging Jet*

1. Introduction

Impinging jets are flow systems where an ejector is used to create a high speed free surface flow (jet), which impinges against an obstacle. Near the collision plate, velocity gradients tend to be very high, favoring localized mass and heat transfer. These jets are widely used in industry, mostly as devices to promote and control localized heat and mass transfer. Common industrial applications for impinging jets are cooling of metals in syderurgics, glass tempering and ventilation of electrical components. Since most applications uses air and water as the cooling fluid due to their relatively low viscosity, flow velocity tends to be high and the study of impinging jets in turbulent regime becomes necessary.

There are several studies about turbulent impinging jets in literature, like the work of Baydar (1999), that experimentally evaluated the hydrodynamics characteristics of single and double jets colliding against a plate. Chalupa et al. (2001) analyzed the mass transference induced by a bidimensional turbulent jet and Park et al. (2003) made a comparison between different numerical methods in flow resolution for both laminar and turbulent regimes.

The study of porous medium is relatively recent, being extensively analyzed on the last decade by its great potential in technological applications, mostly on thermal equipment.

Thermal performance of porous media was studied by Vafai et al (1990), which evaluated heat transfer characteristics of a hybrid medium. Huang and Vafai (1993) analyzed the heat transfer though a flat plate covered with a porous layer. Effects of the insertion of a porous medium in a flow were evaluated by Hadim (1994) that investigated the flow of a channel both fully and partially filled with a porous insert. The study of porous medium under impinging jets are yet very scarce in literature, being examples the work of Prakash et al (2001), which made an experimental and numerical study of turbulent jets impinging against a porous layer. Further, Fu et al (1997) evaluated the thermal performance of different porous media under an impinging jet.

The objective of the present work is to apply the methodology proposed by Pedras and de Lemos (2000,2001) to investigate turbulent impinging jets onto a porous material.

2. Physical Model

The physical model utilized is showed in Fig. (1), representing a cylinder where the jet will collide. At the upper section of the cylinder, there is a disc with a central clearance, where inlet fluid comes from. There’s also an annular clearance between the cylinder and the disc, through exit flow passes. The jet diameter, D_j , is 0.019 m and the inner cylinder diameter, D, is 0.39m. The clearance between the cylinder and the disc holding the jet has a width, w, of 0.005m. Three different heights of fluid column, H, 0.05, 0.1 and 0.15m were used for numerical simulations. The thickness of the porous layer, h_p , placed above the lower plate of the cylinder, assumed two different values for porous medium runs, being it 0.05 or 0.1m. A jet exit average velocity of 1.6 m/s was used as default value for simulations, representing a Reynolds number of 30000, based on jet exit diameter. Different velocities were used only when evaluating influence of Reynolds number on the main flow, being these values 1.0 and 2.5 m/s, representing Re = 18900 and 47000, respectively.

The computational domain adopted for numerical simulations covered half of the cylinder, where an axisymmetric condition was used at the z axis. Simulations were carried with a High Reynolds turbulence model. A fully developed velocity profile was assumed at jet exit. A computational grid of 100 x 100 (10000 nodes) was used for the numerical runs.

Turbulent results for streamfunctions, velocity and turbulence kinetic energy profiles have been compared with literature results from Prakash et al (2001).

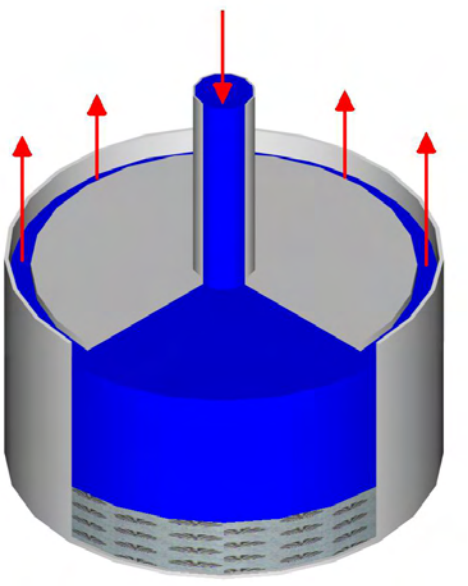

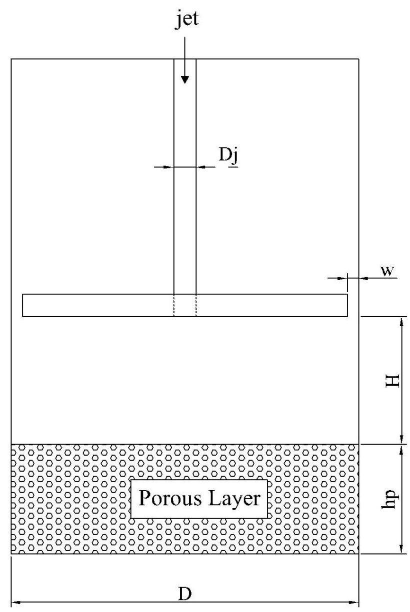

Figure 1 – Physical model : jet impinging against a cylinder covered with a porous layer

3. Mathematical Model

The mathematical model employed in this paper takes account of a series of concepts defined in the works of Pedras and de Lemos (2000,2001), such as intrinsic volumetric average, spatial deviation, the local volumetric average theorem (TMVL) and the double decomposition concept. The implementation of the jump condition at the interface between clear and porous medium was considered in the work of Silva and de-Lemos (2002). Nevertheless, for the sake of simplicity, in this work no jump condition is considered. Therefore, these equations will be reproduced here and details about their derivations can be obtained in the mentioned papers. In this development, it is assumed a homogeneous, rigid porous medium saturated in an incompressible single-phase flow. Also, all physical properties are kept fixed.

3.1 Macroscopic continuity equation

The macroscopic continuity equation can be written as

$$\nabla.\mathbf{u}_D = 0 \tag{1}$$

where $\mathbf{u}_D$ is the average surface velocity (also known as Darcy velocity). In Eq. (1) the Dupuit-Forchheimer relationship, $\overline{\mathbf{u}}_D = \phi\langle\overline{\mathbf{u}}\rangle^i$, has been used, where ϕ is the porous medium porosity and $\langle\overline{\mathbf{u}}\rangle^i$ identifies the intrinsic (volume-averaged on fluid phase) average of the local velocity vector $\overline{\mathbf{u}}$ (Gray and Lee (1977)).

3.2 Macroscopic momentum equation:

The macroscopic momentum equation is given by,

$$\rho\left[\frac{\partial\overline{\mathbf{u}}_D}{\partial t} + \nabla\cdot\left(\frac{\overline{\mathbf{u}}_D\overline{\mathbf{u}}_D}{\phi}\right)\right] = -\nabla\left(\phi\langle\overline{p}\rangle^i\right) + \mu\nabla^2\overline{\mathbf{u}}_D + \nabla\cdot\left(-\rho\phi\langle\overline{\mathbf{u}'\mathbf{u}'}\rangle^i\right) - \left[\frac{\mu\phi}{K}\overline{\mathbf{u}}_D + \frac{c_F\phi\rho|\overline{\mathbf{u}}_D|\,\overline{\mathbf{u}}_D}{\sqrt{K}}\right], \tag{2}$$

where $-\rho\phi\langle\overline{\mathbf{u}'\mathbf{u}'}\rangle^i$ is the macroscopic Reynolds Tensor, given by:

$$-\rho\phi\langle\overline{\mathbf{u}'\mathbf{u}'}\rangle^i = \mu_{t_\phi}2\langle\overline{\mathbf{D}}\rangle^v - \frac{2}{3}\phi\rho\langle k\rangle^i\mathbf{I} \tag{3}$$

where

$$\langle \overline{\mathbf{D}} \rangle^v = \frac{1}{2}\left[\nabla(\phi\langle \overline{\mathbf{u}} \rangle^i) + [\nabla(\phi\langle \overline{\mathbf{u}} \rangle^i)]^T\right] \tag{4}$$

is the macroscopic deformation rate, $\langle k^i \rangle$ is the mean intrinsic volumetric kinetic energy per mass unit and μ_{t_ϕ} is the macroscopic turbulent viscosity, defined as:

$$\mu_{t_\phi} = \rho c_\mu \frac{\langle k \rangle^{i\,2}}{\langle \varepsilon \rangle^i} \tag{5}$$

where c_μ is an adimensional constant. To obtain μ_{t_ϕ}, knowledge of the turbulent kinetic energy intrinsic volumetric average is necessary, $\langle k^i \rangle$, and its dissipation rate, $\langle \varepsilon \rangle^i$, both obtained from transport equations.

3.3 Macroscopic Equation for k and ε :

The macroscopic transport equation for $\langle k \rangle^i = \langle \overline{\mathbf{u}' \cdot \mathbf{u}'} \rangle^i / 2$ is given by,

$$\rho\left[\frac{\partial}{\partial t}\left(\phi\langle k \rangle^i\right) + \nabla \cdot \left(\overline{\mathbf{u}}_D \langle k \rangle^i\right)\right] = \nabla \cdot \left[\left(\mu + \frac{\mu_{t_\phi}}{\sigma_k}\right)\nabla\left(\phi\langle k \rangle^i\right)\right] - \rho\langle \overline{\mathbf{u}'\mathbf{u}'} \rangle^i : \nabla \overline{\mathbf{u}}_D + c_k \rho \frac{\phi \langle k \rangle^i |\overline{\mathbf{u}}_D|}{\sqrt{K}} - \rho\phi\langle \varepsilon \rangle^i \tag{6}$$

where c_k and σ_k are adimensional constants.

The macroscopic equation for $\langle \varepsilon \rangle^i = \mu \langle \overline{\nabla \mathbf{u}' : (\nabla \mathbf{u}')^T} \rangle^i / \rho$ is obtained from the microscopic equation for ε, by applying the volumetric average operator, conducting to the following equation:

$$\rho\left[\frac{\partial}{\partial t}\left(\phi\langle \varepsilon \rangle^i\right) + \nabla.\left(\overline{\mathbf{u}}_D \langle \varepsilon \rangle^i\right)\right] = \nabla.\left[\left(\mu + \frac{\mu_{t_\phi}}{\sigma_\varepsilon}\right)\nabla\left(\phi\langle \varepsilon \rangle^i\right)\right] + c_1\left(-\rho\langle \overline{\mathbf{u}'\mathbf{u}'} \rangle^i : \nabla \overline{\mathbf{u}}_D\right)\frac{\langle \varepsilon \rangle^i}{\langle k \rangle^i} + c_2 c_k \rho \frac{\phi\langle \varepsilon \rangle^i |\overline{\mathbf{u}}_D|}{\sqrt{K}} - c_2 \rho\phi \frac{\langle \varepsilon \rangle^{i\,2}}{\langle k \rangle^i} \tag{7}$$

where c_1, c_2 and c_k are empirical adimensional constants.

3.4 Boundary conditions and model constants

At the jet exit, a fully developed profile for velocity, k and ε was imposed. At flow outlet, a zero diffusion flux condition was set. On the walls, a non-slip condition was applied. An axisymmetric condition was used at the centerline of the cylinder.

The constants of the standard k-ε turbulence model in Eqs 5, 6, 7, according to Launder & Spalding (1974) for a clear medium (ϕ=1 and $K \to \infty$) utilizing a High Reynolds formulation are given by:

$$c_\mu = 0.09, c_1 = 1.44, c_2 = 1.92, \sigma_k = 1.0, \sigma_\varepsilon = 1.33 \tag{8}$$

3.5 Interface condition between clear and porous medium

To obtain the numerical solution of the macroscopic equations, the continuity conditions for macroscopic velocity, intrinsic pressure, turbulence kinetic energy and its dissipation rate, as well as its respective diffusive fluxes were granted by using interface boundary conditions, defined as follows:

$$\overline{\mathbf{u}}_D\big|_{0<\phi<1} = \overline{\mathbf{u}}_D\big|_{\phi=1} \tag{9}$$

$$\langle \overline{p} \rangle^i\big|_{0<\phi<1} = \langle \overline{p} \rangle^i\big|_{\phi=1} \tag{10}$$

$$\langle k\rangle^v\Big|_{0<\phi<1} = \langle k\rangle^v\Big|_{\phi=1} \tag{11}$$

$$(\mu + \frac{\mu_{t_\phi}}{\sigma_k})\frac{\partial\langle k\rangle^v}{\partial y}\Bigg|_{0<\phi<1} = (\mu + \frac{\mu_t}{\sigma_k})\frac{\partial\langle k\rangle^v}{\partial y}\Bigg|_{\phi=1} \tag{12}$$

$$\langle \varepsilon\rangle^v\Big|_{0<\phi<1} = \langle \varepsilon\rangle^v\Big|_{\phi=1} \tag{13}$$

$$(\mu + \frac{\mu_{t_\phi}}{\sigma_\varepsilon})\frac{\partial\langle \varepsilon\rangle^v}{\partial y}\Bigg|_{0<\phi<1} = (\mu + \frac{\mu_t}{\sigma_\varepsilon})\frac{\partial\langle \varepsilon\rangle^v}{\partial y}\Bigg|_{\phi=1} \tag{14}$$

4. Numerical Method

The numerical method utilized to solve the flow equations is the finite volume method applied to a boundary-fitted coordinate system. Equations were discretized in a two-dimensional control volume involving both clear and porous media. For the resolution of the equations the SIMPLE algorithm was used, described in Patankar (1980). The interface is positioned to coincide with the border between two control volumes, generating, in such a way, only volumes of the types 'totally porous' or 'totally clear'. The flow equations are then resolved in the porous and clear domains, considering the interface conditions mentioned earlier. Details of the numerical implementation can be seen in Pedras and de Lemos(2001b), and Silva and de-Lemos (2002). Concerning the convergence criteria, each iteration residues for transport equations have been kept under 10^{-6} .

5. Results and Discussion

For the porous medium cases, a porous layer of defined thickness h_p has been placed over the cylinder base, so that the impinging flow would collide normally to it. For presented cases, a porous layer of two different thickness was used, giving h_p = 0.10 and 0.05m

Porous medium properties used for numerical runs are given on Tab. (1), being these values the same from metallic porous foam utilized in the works of Prakash et al (2001). The porosity of all porous foams considered is very close to unity, so that the change of the porous medium material effectively represents a change in its permeability. The name of the foam came from its number of pores per inch, ppi

Table 1 – Porous medium properties for simulated foams.

Foam	G10	G30	G45	G60
ϕ	0.971	0.9755	0.978	0.976
K (m²)	2.84E-7	6.95E-8	1.6E-8	1.2E-8
c_F (m)	0.1227	0.1218	0.1232	0.1161

5.1 Vector Plots and Streamlines

Figure (2) show a comparison of the numerically simulated streamfunctions with experimental flow visualizations and CFD data from Prakash et al (2001) for H = 0.10m, h_p = 0.05 m and Re = 30000 on porous foam G10. From the picture can be noticed the presence of two big recirculations dominating the entire flow. Aiming for a better organization of results, the recirculation closer to cylinder centerline will be called primary one and the vortice closer to cylinder wall will be named secondary recirculation. For the present case, both primary and secondary recirculations seem to be a little bigger than flow visualizations with LDV, but in a general manner, results seem to be in good agreement with experimental literature data for the entire computational domain. The streamlines inside the porous medium, even tough they cannot be seen by flow visualization methods due to the opaque characteristic of the porous medium, can be well predicted from the flow behavior at the fluid layer section.

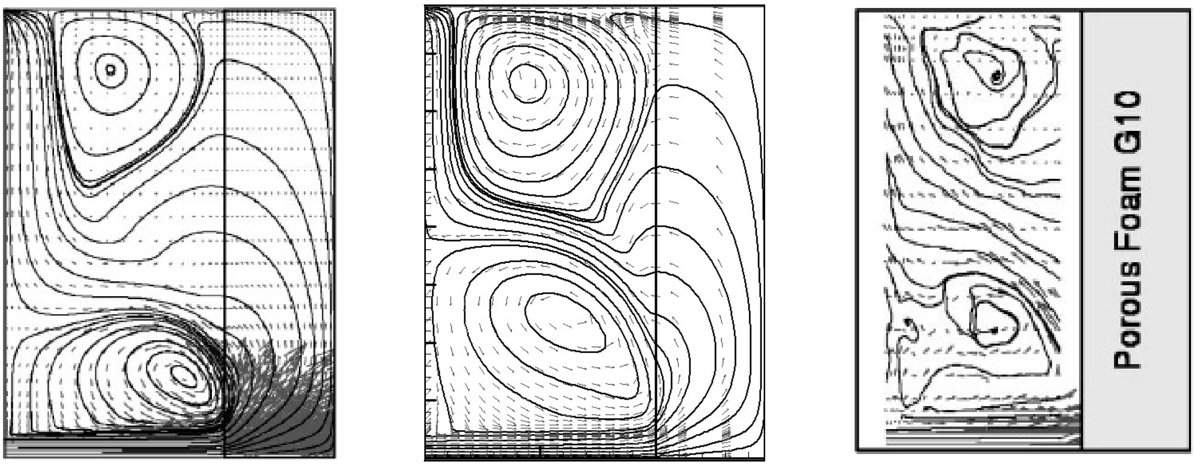

(a) (b) (c)

Figure 2 – Comparison of streamfunctions for H = 0.10m, hp = 0.05m and porous foam G10 (a) CFD Results -Prakash *et al* (2001) (b) Present Results (c) LDV Measurements - Prakash *et al* (2001)

The effect of the fluid layer height, H, is given by fig.(3), showing the streamfunctions for H = 0.15, 0.10 and 0.05m. For H = 0.15m, the primary recirculation is much bigger than the secondary one, indicating a smaller effect of jet penetration into the porous layer, so that flow behavior tends to results from simulations in a cylinder without the presence of the porous layer. This happens due to the spread of the jet before colliding into the porous foam. With a decrease in H, primary recirculation tends to decrease its size as the secondary one grows, so that for H = 0.10m both recirculations have almost same dimensions, filling almost completely the fluid layer and compressing the exit flow streamlines between both recirculations. For H = 0.05m, both recirculations decrease their size, moving their center into the cylinder centerline for primary bubble and cylinder wall for the secondary one. Streamlines between both recirculations are distributed rather regularly, with no significant change in flow direction as it leaves porous media to the fluid layer, unlike streamlines behavior for higher values of H.

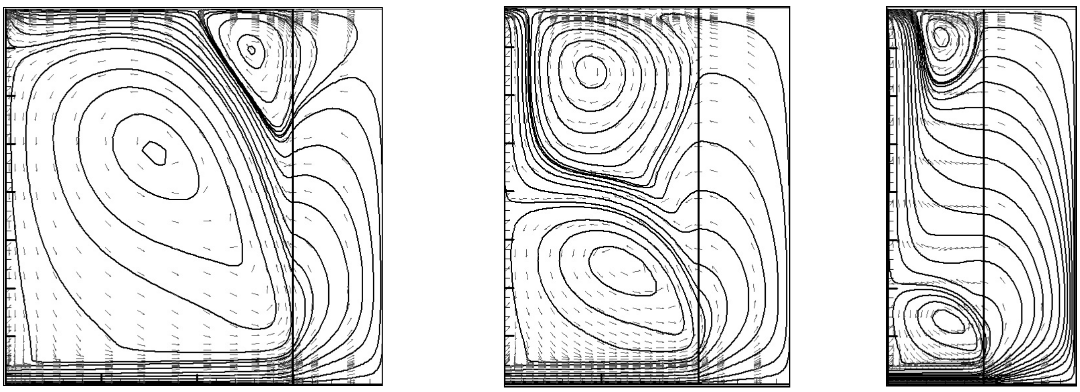

(a) (b) (c)

Figure 3 – Effect of the fluid layer height on streamfunctions for hp= 0.05m, Re = 30000 and porous foam G10 (a) H = 0.15m (b) H = 0.10m (c) H = 0.05m

The effect of the porous layer thickness, h_p, is showed on Fig. (4). From the picture, it can be seen that this parameter has a minor influence in the main flow behavior in comparison to the fluid layer height, H. With an increase in h_p, primary recirculation show a small increase in size while the secondary one decreases a little, but no other significant difference could be detected.

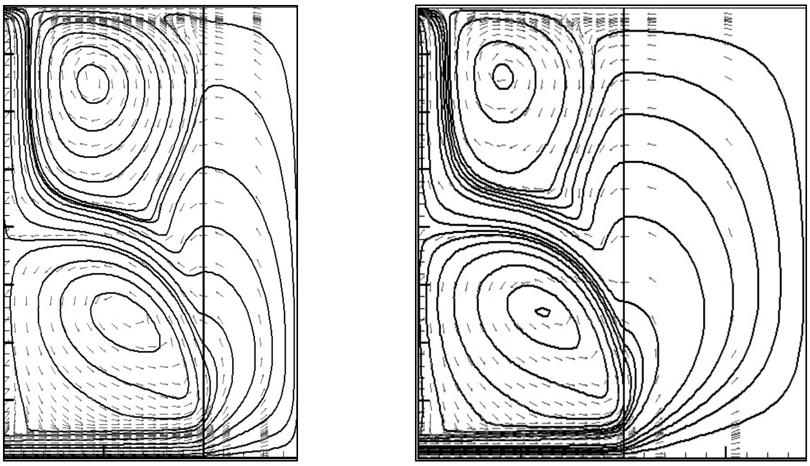

(a) (b)

Figure 4 – Effect of the porous layer thickness on streamfunctions for H= 0.10m, Re = 30000 and porous foam G10 (a) hp = 0.05m (b) hp = 0.10m

The effect of the porous layer material, effectively representing a change in its permeability, can be well discerned by Fig. (5). For the porous foam G10 with the highest permeability, a secondary recirculation develops with considerable size close to the cylinder wall. For porous foams G30, G45 and G60, this recirculation decreases with the decrease of the porous layer permeability, so that the porous layer tends to act as a solid obstacle to the jet.

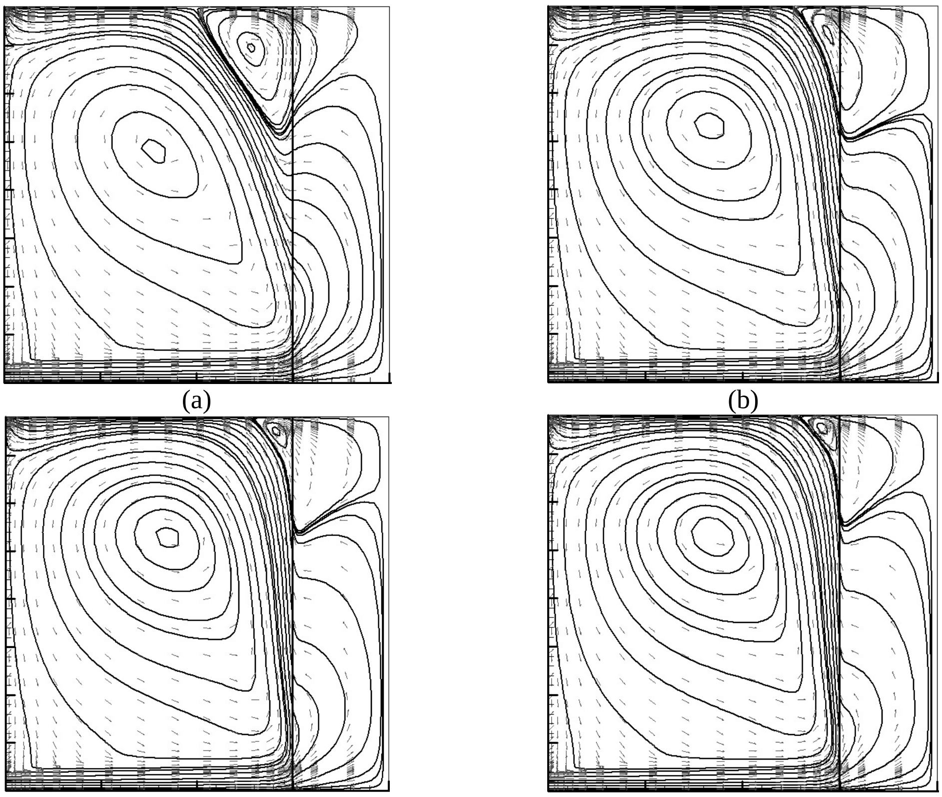

(a) (b) (c) (d)

Figure 5 – Effect of porous medium material on streamfunctions for H = 0.15m, hp = 0.05m on different porous (a) Porous Foam G10 (b) Porous Foam G30 (c) Porous Foam G45 (d) Porous Foam G60

Figure (6) gives the Reynolds number influence on the flow pattern. Like results for the clear medium section, a change in Re doesn't apply a significant influence in the flow pattern, for both the porous and fluid layer.

Copyright © 2005 by ABCM

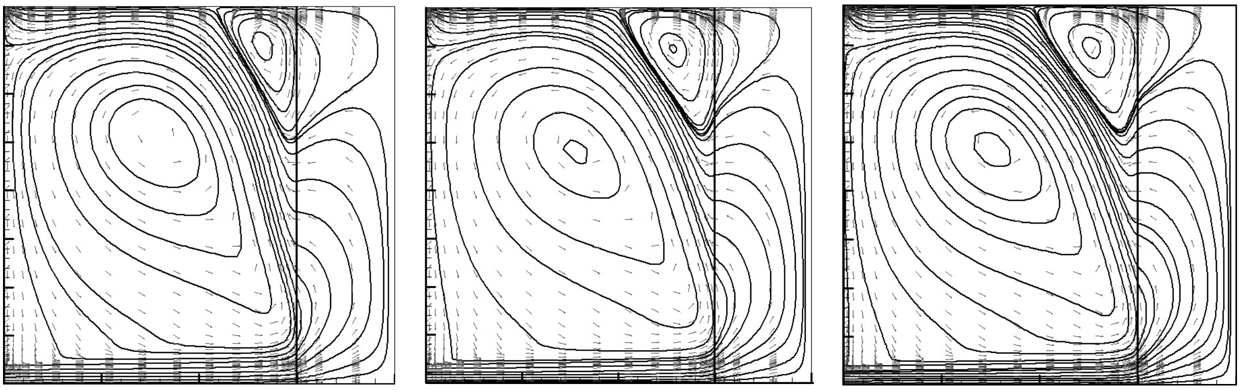

Figure 6 – Effect of Reynolds number on streamfunctions for H = 0.15m, hp = 0.05m on porous foam G10 (a) Re = 18900 (b) Re = 30000 (c) Re = 47000

5.2 Turbulent Kinetic Energy Contours

Figure (7) show turbulent kinetic energy contours comparisons for h_p = 0.05 m on porous foam G10 and Re = 30000. From the picture, it can be seen that turbulence penetrates the porous medium, as can be noticed by the contour lines that goes inside the porous bed. The damping of the turbulence in the present model seems to be lower than results from Prakash et al (2001) utilizing only the Darcy term (TM1), given by the dashed lines in Fig. (7b), but higher than results using both Darcy and Forchheimer term (TM2), represented by the solid lines, where turbulence is damped almost completely at the interface. At the fluid layer, present results are in accord with theoretical expectations.

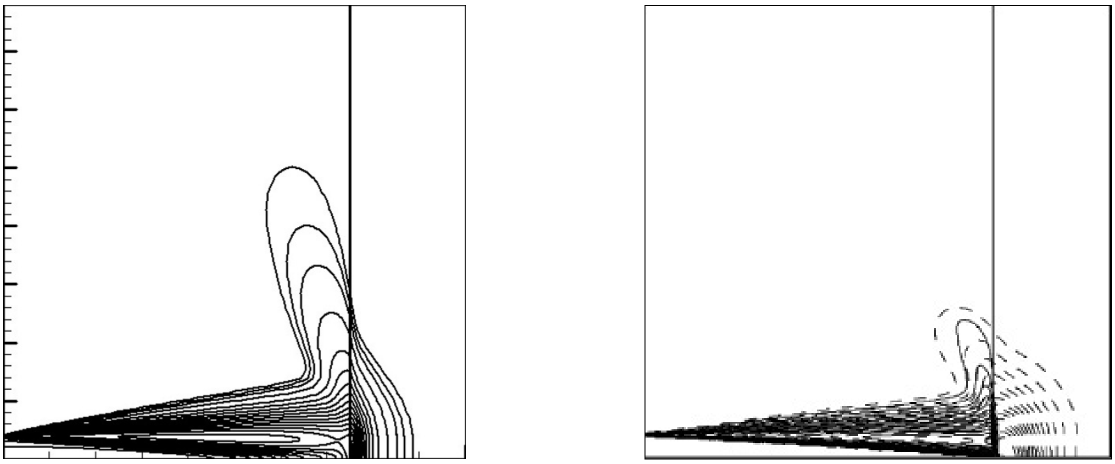

Figure 7 – Comparison of turbulence kinetic energy contours for H = 0.15m, hp = 0.05m on porous foam G10 (a) Present Results (b) CFD Results -Prakash *et al* (2001)

6. Conclusions and Recommendations

For numerical simulations, some variables were analyzed to measure its effect in the flow, being these parameters the Reynolds number, porous layer height, fluid layer height and material of the porous medium itself, incorporating both porosity and permeability simultaneous variation. Since the porosity for all foams utilized was very close do unity, the change in the foam material can be described as a change in its permeability only. It was observed that the permeability of the porous layer and the height of the fluid layer significantly affect the flow pattern, with a lesser effect from the porous layer thickness. The effect of the Reynolds number to the flow behavior is very small, indicating a fully turbulent regime. Comparisons with literature data indicate that the turbulence model utilized well describes the turbulence phenomena inside a porous medium.

7. Acknowledgments

The authors are thankful to CNPq and FAPESP, Brazil, for their financial support during the course of this research.

8. References

Baydar, E., 1999, “Confined Impinging Air Jet at Low Reynolds Numbers”, Experimental Thermal and Fluid Science, 19, pp. 27-33.

Chalupa, R., Chen., M., West, A.C., Modi, V., 2001, “High Schmidt Mass Transfer in a Turbulent Impinging Slot Jet”, International Journal of Heat and Mass Transfer, 44, pp. 3775-3785.

Park, T.H., Choi., H.G., Yoo, J.Y., Kim, S.J., 2003, “Streamline Upwind Numerical Simulation of Two-Dimensional Confined Impinging Slot Jets”, International Journal of Heat and Mass Transfer, Vol. 46, pp. 251-262.

Vafai, K., Kim, S.J., 1990, “Analysis of surface enhancement by a porous substrate”, Journal of Heat Transfer, 112, 700-706.

Huang, P.C., Vafai, K., 1993, “Flow and heat transfer control over an external surface using a porous block array arrangement.” International Journal of Heat and Mass Transfer, 36, 4019-4032.

Hadim, A., 1994, “Forced convection in a porous channel with localized heat sources”, Journal of Heat Transfer, 116, 465-472.

Prakash, M., Turan, F.O., Li, Y., Manhoney, J., Thorpe, G.R., 2001, Impinging Round Jet Studies In A Cilindrical Enclosure With And Without A Porous Layer: Part I: Flow Visualisations And Simulations, Chemical Engrg Science, Vol.56, pp. 3855-3878

Prakash, M., Turan, F.O., Li, Y., Manhoney, J., Thorpe, G.R., 2001, Impinging Round Jet Studies In A Cilindrical Enclosure With And Without A Porous Layer: Part II: DLV Measurements And Simulations, Chemical Engrg Science, Vol.56, pp. 3879-3892

Fu, W.-S., Huang, H.,-C, 1997, “Thermal performance of different shape porous blocks under an impinging jet”, International Journal of Heat and Mass Transfer, Vol. 40, No. 10, pp. 2261-2272.

Pedras, M.H.J., de Lemos, M.J.S., 2000, On the Definition of Turbulent Kinetic Energy for Flow in Porous Media, Intern. Comm. Heat and Mass Transfer, 27(2), 211-220.

Pedras, M.H.J., de Lemos, M.J.S., 2001, “Macroscopic Turbulence Modeling For Incompressible Flow Through Undeformable Porous Media”, Int. J. Heat Transfer, vol 44, n. 6, pp. 1081-1093.

Pedras, M.H.J., de Lemos, M.J.S., 2001, “Simulation of Turbulent Flow in Porous Media Using a Spatially Periodic Array and a Low Re Two-Equation Closure”, Numer. Heat Transfer Part A-Appl, vol. 39, n. 1, pp. 35-59.

Gray, W.G., Lee, P.C.Y., 1977. On the theorems for local volume averaging of multiphase system. Int. J. Multiphase Flow, vol.12, pp.401-410.

Patankar, S.V., 1980, “Numerical Heat Transfer and Fluid Flow”, Hemisphere, New York.

Launder, B.E. & Spalding, D.B., 1974, The Numerical Computation of Turbulent Flows, *Comp. Meth. Appl. Mech. Eng.*, vol. 3, pp. 269-289

Silva, R.A., de-Lemos, M.J.S., 2002, “Numerical Treatment of the Stress Jump Interface Condition for Laminar Flow in a Channel Containing a Porous Layer”, *Numerical Heat Transfer – Part A.*